Journal of Marine Science and Technology

Volume 21 | Issue 4 Article 2

SHAPE OPTIMIZATION OF ONE-CHAMBER PERFORATED MUFFLERS FILLED WITH WOOL USING SIMULATED ANNEALING

Min-Chie Chiu
Department of Mechanical and Automation Engineering, Chun Chiu University of Science and Technology, Changhua County, Taiwan, R.O.C., minchie.chiu@msa.hinet.net

Recommended Citation
Chiu, Min-Chie (2013) "SHAPE OPTIMIZATION OF ONE-CHAMBER PERFORATED MUFFLERS FILLED WITH WOOL USING SIMULATED ANNEALING," *Journal of Marine Science and Technology*: Vol. 21: Iss. 4, Article 2.
DOI: 10.6119/JMST-012-0517-1
Available at: https://jmstt.ntou.edu.tw/journal/vol21/iss4/2

SHAPE OPTIMIZATION OF ONE-CHAMBER PERFORATED MUFFLERS FILLED WITH WOOL USING SIMULATED ANNEALING

Acknowledgements

The author acknowledges the financial support of the National Science Council (NSC99-2221-E-235-001, Taiwan, ROC)

Journal of Marine Science and Technology, Vol. 21, No. 4, pp. 380-390 (2013)
DOI: 10.6119/JMST-012-0517-1

SHAPE OPTIMIZATION OF ONE-CHAMBER PERFORATED MUFFLERS FILLED WITH WOOL USING SIMULATED ANNEALING

Min-Chie Chiu

Key words: space constraints, dissipative muffler, wool, simulated annealing.

ABSTRACT

Research on dissipative and reactive mufflers has been addressed. However, the acoustical performance —sound transmission loss (*STL*)— of mufflers within a constrained space is often insufficient. In this paper, to improve the acoustical efficiency, a one-chamber perforated muffler filled with sound absorbing wool optimized by using simulated annealing (*SA*) in conjunction with the numerical decoupling technique is presented. A numerical case in eliminating a broadband noise is also introduced. To verify the reliability of *SA* optimization, optimal noise abatements for the pure tone are exemplified. Before the *SA* operation can be carried out, the accuracy of the mathematical models has been checked using the experimental data. Results indicate that the maximal *STL* is precisely located at the desired target tone. Moreover, the *STL* can be improved when the ratio of the perforated tube's length and the porosity of the perforated tube and the acoustical flowing resistance of the wool increase and the Mach number and the expansion ratio decrease. Consequently, a successful approach used for the optimal design of the one-chamber dissipative mufflers within a constrained space has been demonstrated.

I. INTRODUCTION

Research on mufflers used in reducing high frequency noise using a duct lined with sound absorbing material was started by Morse in 1939 [10]. Scott [17] used a volume model in solving the acoustical performance in both the circular and rectangular duct lined with porous material. Ko [7] assessed the sound transmission loss in acoustically lined flow ducts separated by porous splitters in 1975. Cummings and Chang [3] investigated the duct's acoustical performance at various mean flows using the characteristics of bulk-reacting liners in circular ducts. On the basis of an infinite duct, the above researches analyzed the acoustical performance of the duct at a fixed duct's diameter. Cummings and Chang [4] developed a modal method in analyzing a finite length dissipative flow duct silencer with internal mean flow in the absorbent in 1988. Regarding the volume modulus, Peat [15], in 1991, used a transfer matrix in evaluating the acoustical performance for an absorption silencer element. Selamet *et al*. [18, 19] assessed the acoustical attenuation for perforated concentric absorbing silencers and hybrid silencers using a one-dimensional analytical method, a three-dimensional boundary element method (BEM), and an experimental study. Wang proposed a three-dimensional boundary element method (BEM) in analyzing the acoustical performance of a one-chamber dissipative muffler [24]. By way of plane wave theory, Munjal [12], in 2003, proposed a four-pole transfer matrix in solving the sound attenuation of pod silencers lined with porous material. Xu *et al*. [25] assessed the sound attenuation in dissipative expansion chambers using the characteristic equation in 2004. However, the assessment of a muffler's optimal shape design within a constrained space was rarely tackled.

In previous work [1, 2], the shape optimization of one-chamber mufflers equipped with a perforated resonating tube within a constrained situation has been discussed. However, its acoustical performance is insufficient in dealing with a higher and broader frequency noise because of the characteristic narrow band effect. To improve acoustical efficiency, an assessment of one-chamber perforated mufflers lined with porous material is presented.

An assessment of a perforated acoustical element used to depress low frequency sound energy was introduced and discussed by Sullivan and Crocker in 1978 [22]. On the basis of the coupled differential equations, a series of theoretical and numerical techniques in decoupling the acoustical problems have been proposed [5, 13, 16, 20, 21, 23]. Peat [14] publicized a successfully numerical decoupling method by finding the eigen value in transfer matrices. Here, the numerical

Paper submitted 06/11/11; revised 01/14/12; accepted 05/17/12. Author for correspondence: Min-Chie Chiu (e-mail: minchie.chiu@msa.hinet.net).
Department of Mechanical and Automation Engineering, Chun Chiu University of Science and Technology, Changhua County, Taiwan, R.O.C.

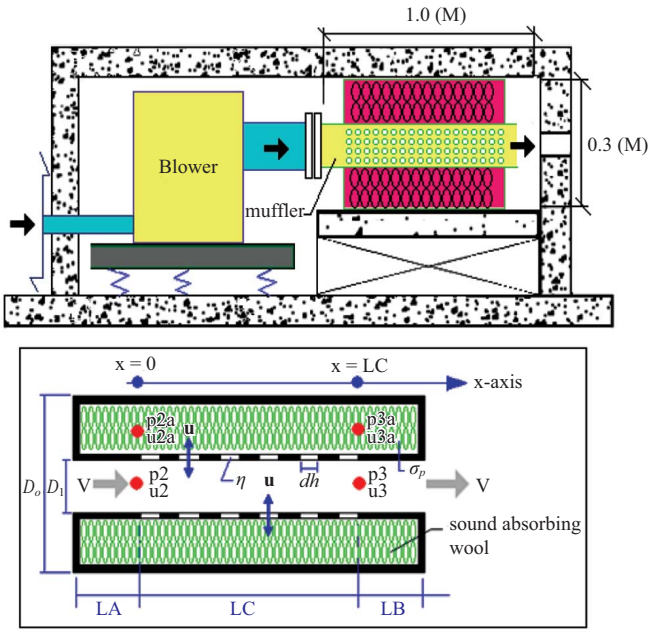

Fig. 1. A blower equipped with a muffler within a constrained room.

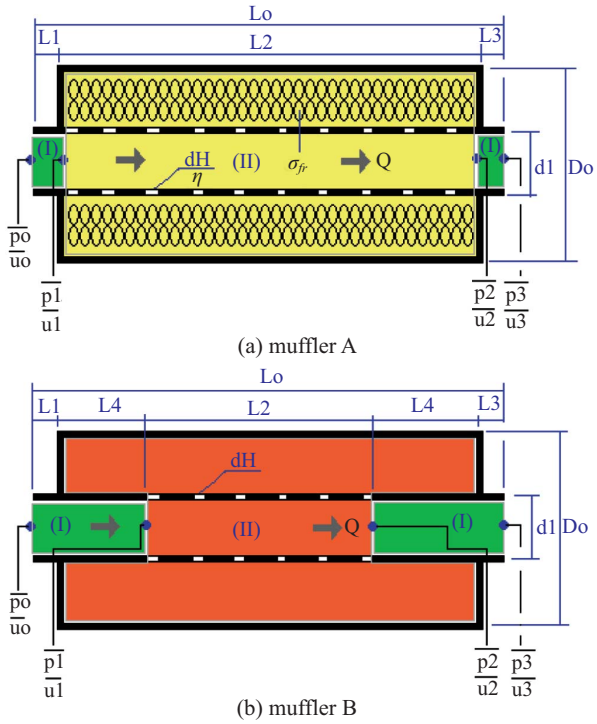

Fig. 2. The outlines and related acoustic pressure *p* and acoustic particle velocity *u* and recognition of acoustical elements for the mufflers: (a) muffler A is filled with sound absorption wool and (b) muffler B is empty chamber.

decoupling methods used in forming a four-pole system matrix are in line with the simulated annealing (*SA*) method. These, in turn, are responsible for developing a new muffler shape by adjusting the geometric parameters (i.e., the length of the dissipative muffler, the porosity of the inner duct, the diameter of the perforated hole on the inner duct, and the diameter of the inner duct) and the acoustical property of the wool (i.e., the wool's acoustical flowing resistance) within certain space constraints. To appreciate the acoustical performance with/without sound absorbing wool, a one-chamber perforated muffler without sound absorbing wool is also numerically assessed.

II. THEORETICAL BACKGROUND

In this paper, two one-chamber perforated mufflers with and without sound absorbing material were adopted for the noise abatement in the constrained blower room shown in Fig. 1. The outlines and recognition of acoustical elements and the related acoustic pressure *p* and acoustic particle velocity *u* for various mufflers is depicted in Fig. 2.

As indicated in Fig. 2(a), the one-chamber perforated muffler (muffler A) filled with wool and composed of three acoustical elements is identified as having two categories of components — two straight ducts (I) and one perforated dissipative chamber (II). Fig. 2(b) indicates that the one-chamber muffler (muffler B) hybridized with a perforated resonating tube composed of three acoustical elements is identified as having two categories of components — two straight ducts (I) and one perforated resonating tube (II). The detailed mathematical derivation of various muffler systems is presented below.

1. A One-chamber Muffler with Sound Absorbing Material (Muffler A)

As shown in Appendix A, the transfer matrix of a perforated chamber filled with sound absorbing wool is derived. The individual matrixes with respect to straight ducts and a perforated resonating tube are described as follows [1, 2]:

$$\begin{pmatrix} \bar{p}_1 \\ \rho_o c_o \bar{u}_1 \end{pmatrix} = e^{-jM_1 kL_1/(1-M_1^2)} \begin{bmatrix} TS11_{1,1} & TS11_{1,2} \\ TS11_{2,1} & TS11_{2,2} \end{bmatrix} \begin{pmatrix} \bar{p}_2 \\ \rho_o c_o \bar{u}_2 \end{pmatrix} \quad (1)$$

$$\begin{pmatrix} \bar{p}_2 \\ \rho_o c_o \bar{u}_2 \end{pmatrix} = \begin{bmatrix} TPD12_{1,1} & TPD12_{1,2} \\ TPD12_{2,1} & TPD12_{2,2} \end{bmatrix} \begin{pmatrix} \bar{p}_3 \\ \rho_o c_o \bar{u}_3 \end{pmatrix} \quad (2)$$

$$\begin{pmatrix} \bar{p}_3 \\ \rho_o c_o \bar{u}_3 \end{pmatrix} = e^{-jM_1 kL_3/(1-M_1^2)} \begin{bmatrix} TS13_{1,1} & TS13_{1,2} \\ TS13_{2,1} & TS13_{2,2} \end{bmatrix} \begin{pmatrix} \bar{p}_4 \\ \rho_o c_o \bar{u}_4 \end{pmatrix} \quad (3)$$

The total transfer matrix assembled by multiplication is

$$\begin{pmatrix} \bar{p}_1 \\ \rho_o c_o \bar{u}_1 \end{pmatrix} = e^{-jkM_1\left[\frac{L_1+L_3}{1-M_1^2}\right]} \begin{bmatrix} TS11_{1,1} & TS11_{1,2} \\ TS11_{2,1} & TS11_{2,2} \end{bmatrix} \begin{bmatrix} TPD12_{1,1} & TPD12_{1,2} \\ TPD12_{2,1} & TPD12_{2,2} \end{bmatrix} \begin{bmatrix} TS13_{1,1} & TS13_{1,2} \\ TS13_{2,1} & TS13_{2,2} \end{bmatrix} \begin{pmatrix} \bar{p}_4 \\ \rho_o c_o \bar{u}_4 \end{pmatrix} \quad (4)$$

Subsequently, a simplified form of a system matrix for the muffler is expressed as

$$\begin{Bmatrix} \overline{p}_1 \\ \rho_o c_o \overline{u}_1 \end{Bmatrix} = \prod_m \left[T_m(f) \right] \begin{Bmatrix} \overline{p}_4 \\ \rho_o c_o \overline{u}_4 \end{Bmatrix} \quad (5)$$

The sound transmission loss (*STL*) of the muffler A is expressed as [11]

$$STL(Q,\ f, RT_1, RT_2, RT_3, RT_4, RT_5)$$
$$= 20\log\left(\frac{1}{2}(T_{11}+T_{12}+T_{21}+T_{22})\right)+10\log\left(S_1/S_4\right) \quad (6a)$$

where

$$RT_1 = L_2/L_o;\ RT_2 = \sigma_{fr};\ RT_3 = d\mathrm{H};\ RT_4 = \eta;\ RT_5 = d_1/D_o \quad (6b)$$

2. A One-chamber Muffler without Sound Absorbing Material (Muffler B)

As derived in the previous work [1, 2], individual transfer matrixes with respect to straight ducts and a perforated resonating tube are described as follows:

The total transfer matrix assembled by multiplication is

$$\begin{pmatrix} \overline{p}_1 \\ \rho_o c_o \overline{u}_1 \end{pmatrix} = e^{-jkM_1\left[\frac{L_1+L_3+2*L_4}{1-M_1^2}\right]} \begin{bmatrix} TS11_{1,1} & TS11_{1,2} \\ TS11_{2,1} & TS11_{2,2} \end{bmatrix}$$
$$\begin{bmatrix} TPR12_{1,1} & TPR12_{1,2} \\ TPR12_{2,1} & TPR12_{2,2} \end{bmatrix} \begin{bmatrix} TS13_{1,1} & TS13_{1,2} \\ TS13_{2,1} & TS13_{2,2} \end{bmatrix} \begin{pmatrix} \overline{p}_4 \\ \rho_o c_o \overline{u}_4 \end{pmatrix} \quad (7)$$

Subsequently, a simplified form of a system matrix for the muffler is expressed as

$$\begin{Bmatrix} \overline{p}_1 \\ \rho_o c_o \overline{u}_1 \end{Bmatrix} = \prod_m \left[T_m(f) \right] \begin{Bmatrix} \overline{p}_4 \\ \rho_o c_o \overline{u}_4 \end{Bmatrix} \quad (8)$$

The sound transmission loss (*STL*) of the muffler B is expressed as [11]

$$STL(Q,\ f, RT_1^*, RT_2^*, RT_3^*, RT_4^*, RT_5^*)$$
$$= 20\log\left(\frac{1}{2}(T_{11}+T_{12}+T_{21}+T_{22})\right)+10\log\left(S_1/S_4\right) \quad (9)$$

3. Overall Sound Power Level

The overall SWL_T silenced by the muffler at the outlet is

$$SWL_T = 10\log_{10}\left(\sum_m 10^{(SWL(f_m)-STL(f_m))/10}\right) \quad (10)$$

where (1) $SWL(f_m)$ is the original *SWL* at the inlet of the muffler (or pipe outlet), and m is the index of the octave band frequency.

(2) $STL(f_m)$ is the muffler's *STL* with respect to the relative octave band frequency.

4. Objective Function

By using the formulas of Eqs. (6) and (9), the objective function used in the *SA* optimization with respect to each type of muffler was established.

For a one-chamber perforated muffler with sound absorbing wool, the objective function in maximizing the *STL* at the pure tone (f) is

$$OBJ_{11} = STL(f, RT_1, RT_2, RT_3, RT_4, RT_5) \quad (11)$$

The objective function in eliminating the overall SWL_T is

$$OBJ_{12} = SWL_T(RT_1, RT_2, RT_3, RT_4, RT_5) \quad (12)$$

Similarly, for a one-chamber perforated muffler hybridized without sound absorbing wool, the objective function in maximizing the *STL* at the pure tone (f) is

$$OBJ_{21} = STL(f, RT_1^*, RT_2^*, RT_3^*, RT_4^*, RT_5^*) \quad (13)$$

The objective function in eliminating the overall SWL_T is

$$OBJ_{22} = SWL_T(RT_1^*, RT_2^*, RT_3^*, RT_4^*, RT_5^*) \quad (14)$$

III. MODEL CHECK

Before performing the *SA* optimal simulation on mufflers, an accuracy check of the mathematical model on the acoustical elements of one-chamber perforated mufflers with in the chamber are performed using the experimental data from Lee [8]. As depicted in Fig. 3, the theoretical and experimental data are accurate and in agreement. Therefore, the proposed fundamental mathematical models are acceptable. Consequently, the model linked with the numerical method is applied to the shape optimization in the following section.

IV. CASE STUDIES

In this paper, a muffler confined inside a blower room is shown in Fig. 1. The primary noise of the blower's sound power level inside the pipe outlet (muffler's inlet) is listed in Table 1. To efficiently reduce the sound energy, two kinds of mufflers (muffler A: a one-chamber perforated muffler with sound absorbing wool; muffler B: a one-chamber muffler without sound absorbing wool) are adopted. As shown in Fig. 1, the available space for a muffler is 0.3 m in width, 0.3 m in height, and 1.0 m in length. To simplify the optimization,

Table 1. Unsilenced primary *SWL* of a blower inside a duct outlet.

Frequency - Hz	500	1000	2000	overall
SWLO – dB(A)	98	110	123	123

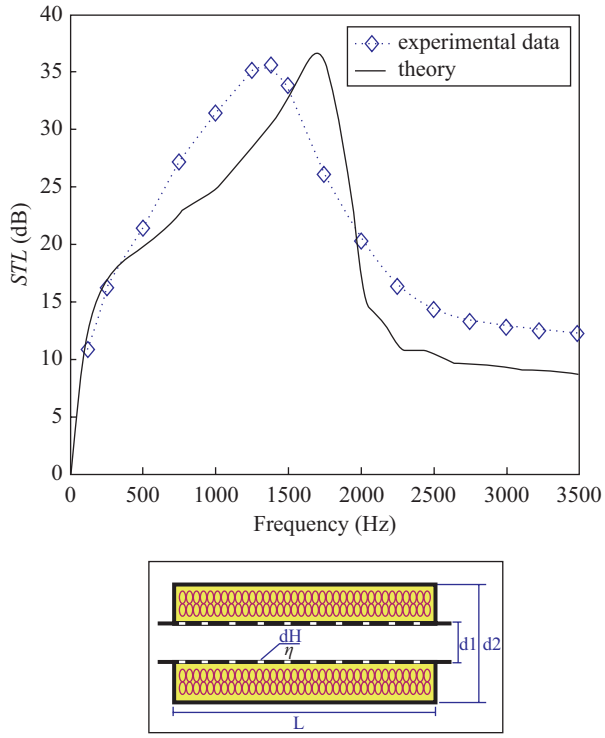

Fig. 3. Performance of a single-chamber dissipative muffler without the mean flow [L = 0.2572(m); $d1$ = 0.00049 (m); $d2$ = 0.001644 (m); η = 8.4%; dH = 0.00498 (m); density = 100 (kg/m^3); M = 0] [Experimental data is from Lee [8]].

the flow rate (Q = 0.01 (m^3/s)) and the thickness of the perforated tube (t = 0.0015 (m)) are preset in advance. The corresponding space constraints and the ranges of the design parameters are summarized in Table 2. Before the minimization of the broadband noise is performed, the maximization of the *STL* at the targeted pure tone (1700 Hz) has been performed for the purpose of an accuracy check on the *SA* method.

V. OPTIMIZATION

The basic concept behind simulated annealing (*SA*) was first introduced by Metropolis *et al.* [9] and developed by Kirkpatrick *et al.* [6]. For a *SA* method, each point X of the search space is compared to a state of some physical system, and the function $F(X)$ to be minimized is interpreted as the internal energy of the system in that state. Therefore, the goal is to bring the system from an arbitrary initial state to a state with the minimum possible energy. Annealing is the process of heating and keeping a metal at a stabilized temperature

Table 2. The corresponding space constraints and the ranges of design parameters for a muffler.

	Range of design parameters
muffler with sound absorption wool (Muffler A)	Targeted f : [1700] (Hz); Q = 0.01 (m^3/s); L_o = 1.0 (m); D_o = 0.3 (m); RT_1: [0.2, 0.8]; RT_2: [4000, 20000]; RT_3: [0.00175, 0.007]; RT_4: [0.03, 0.1]; RT_5: [0.4, 0.8]
muffler without sound absorption wool (Muffler B)	Targeted f : [1700] (Hz); Q = 0.01 (m^3/s); L_o = 1.0 (m); D_o = 0.3 (m); RT_1: [0.03, 0.1]; RT_2: [0.00175, 0.007]; RT_3: [0.4, 0.8]; RT_4: [0.2, 0.8]; RT_5: [0.2, 0.8]

while cooling it slowly. Slow cooling allows the particles to keep their state close to the minimal energy state. The algorithm starts by generating a random initial solution. The scheme of *SA* is a variation of the hill-climbing algorithm. All downhill movements for improvement are accepted for the decrement of the system's energy. In order to escape from the local optimum, *SA* also allows movement resulting in solutions that are worse (uphill moves) than the current solution. To imitate the evolution of the *SA* algorithm, a new random solution (X') is chosen from the neighborhood of the current solution (X). If the change in the objective function (or energy) is negative ($\Delta F \le 0$), the new solution will be acknowledged as the new current solution with the transition property ($pb(X')$ of 1. If the change is not negative ($\Delta F > 0$), the probability of making the transition to the new state X' will be a function $pb(\Delta F/CT)$ of the energy difference $\Delta F = (X') - F(X)$ between the two states and a function of the global time-varying parameter T. The new transition property ($pb(X')$) varied from 0~1 will be calculated by Boltzmann's factor ($pb(X') = \exp(-\Delta F/CT)$) as shown in Eq. (15)

$$pb(X') = \begin{cases} 1, \Delta F \le 0 \\ \exp(\dfrac{-\Delta F}{CT}), \Delta f > 0 \end{cases} \tag{15a}$$

$$\Delta F = F(X') - F(X) \tag{15b}$$

where C and T are the Boltzmann constant and the current temperature. Moreover, compared with the new random probability of rand(0,1), if the transition property ($pb(X')$) is greater than a random number of rand(0,1), the new solution (worse solution) which results in a higher energy condition will then be accepted; otherwise, it is rejected. Each successful substitution of the new current solution will lead to the decay of the current temperature as

$$T_{new} = kk * T_{old} \tag{16}$$

where kk is the cooling rate.

The flow diagram of the *SA* optimization is described and

Table 3. Optimal design data for muffler A at various *SA* parameters (*iter* and *kk*) (targeted tone at 1700 Hz).

SA parameter		Design parameters					Performance
iter	*kk*	RT_1	RT_2	RT_3	RT_4	RT_5	*STL* (dB)
50	0.91	0.3948	9195	0.003455	0.05273	0.5299	19.95
50	0.93	0.4690	11170	0.004104	0.06138	0.5793	29.14
50	0.95	0.4811	11500	0.004209	0.06279	0.5874	31.01
50	0.97	0.5003	12010	0.004377	0.06503	0.6002	34.26
50	0.99	0.5371	12990	0.0047	0.06933	0.6247	41.86
100	0.99	0.5643	13720	0.004938	0.07251	0.6429	49.33
500	0.99	0.6388	15700	0.00559	0.0812	0.6926	72.35
1000	**0.99**	**0.6207**	**15220**	**0.005431**	**0.07908**	**0.6805**	**74.27**

Table 4. Optimal design data for two kinds of mufflers (targeted tone at 1700 Hz) (*iter* = 1000; *kk* = 0.99).

Muffler type	Design parameters					Performance
Muffler A	RT_1	RT_2	RT_3	RT_4	RT_5	STL_{1700} dB(A)
	0.6207	15220	0.005431	0.07908	0.6805	74.27
Muffler B	RT_1^*	RT_2^*	RT_3^*	RT_4^*	RT_5^*	STL_{1700} dB(A)
	0.0826	0.0023	0.4997	0.5271	0.5401	53.61

Notes: $RT_1^* = \eta$; $RT_2^* = dH$; $RT_3^* = d_1/D_o$; $RT_4^* = (L_2 + 2 \cdot L_4)/L_o$; $RT_5^* = L_2/(2 \cdot L_4 + L_2)$

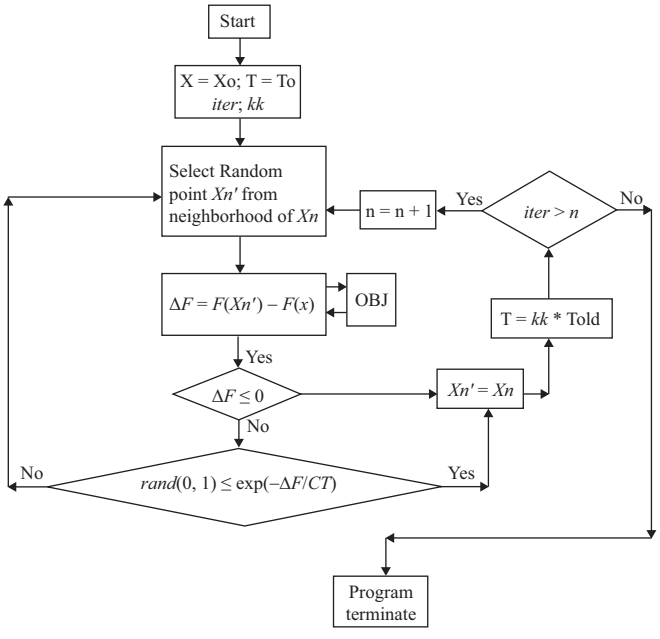

Fig. 4. The flow diagram of the *SA* optimization.

shown in Fig. 4. The process is repeated until the predetermined number (*iter*) of the outer loop is reached. Obviously, the effect of the state energies on the system's evolution depends on the temperature. The evolution is sensitive only to coarser energy variations when *T* is large and to finer variations when *T* is small.

VI. RESULTS AND DISCUSSION

1. Results

The accuracy of the *SA* optimization depends on the cooling rate (*kk*) and the number of iterations (*iter*). To achieve good optimization, both the cooling rate (*kk*) and the number of iterations (*iter*) are varied step by step

kk = (0.91, 0.93, 0.95, 0.97, 0.99); *iter* = (50, 100, 500, 1000)

The results of two kinds of optimizations (one, a pure tone noise; the other, a broadband noise) are described as follows:

1) Pure Tone Noise Optimization

By using Eqs. (6) and (11), the maximization of the *STL* with respect to muffler A at the specified higher pure tone (1700 Hz) was performed first. As indicated in Table 3, eight sets of *SA* parameters are tried in the muffler's optimization.

Obviously, the optimal design data can be obtained from the last set of *SA* parameters at (*kk*, *iter*) = (0.99, 1000). Similarly, by using the *SA* parameters of (*kk* = 0.99, *iter* = 1000) in mufflers A and B, the resultant *STL*s at a targeted tone (1700 Hz) have been summarized in Table 4. Using these optimal design data in a theoretical calculation, the resultant curves of the *STL* with respect to various mufflers are plotted in Fig. 5.

2) Broadband Noise Optimization

By using the formulas of Eqs. (10), (12), and (14) and the *SA* parameters of (*kk* = 0.99, *iter* = 1000), the optimization

Table 5. Optimal design data for two kinds of mufflers (broadband noise) (*iter* = 1000; *kk* = 0.99).

Muffler type	Design parameters					Performance
Muffler A	RT_1	RT_2	RT_3	RT_4	RT_5	*SWL* (dB)
	0.7581	18880	0.003633	0.09511	0.7721	78.51
Muffler B	RT_1^*	RT_2^*	RT_3^*	RT_4^*	RT_5^*	*SWL* (dB)
	0.0775	0.0037	0.4077	0.6259	0.7228	97.52

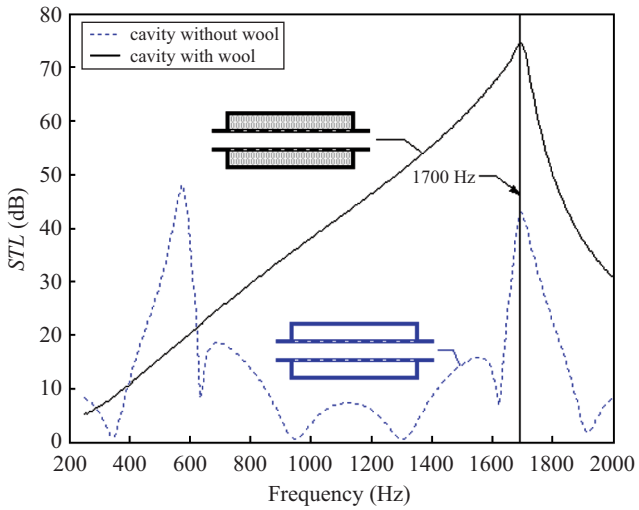

Fig. 5. The *STL* with respect to frequencies at various *kk* (targeted tone: 1700 Hz).

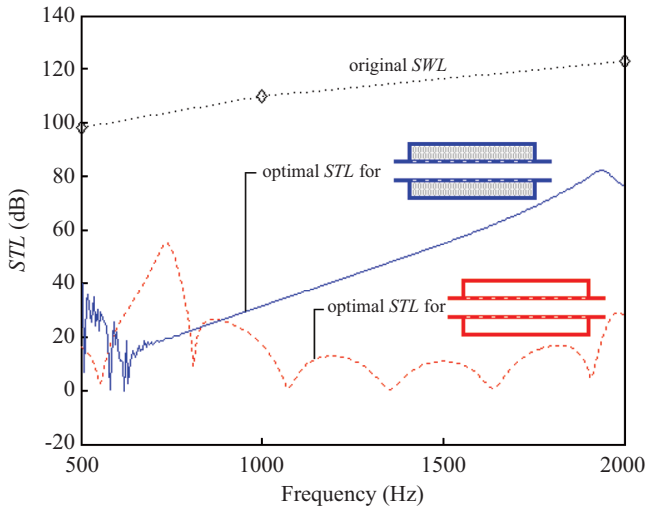

Fig. 6. The *STL* with respect to frequencies at various mufflers (broadband noise).

process for minimizing the sound power level at the muffler's outlet within a limited space is performed. The optimal result at various mufflers is obtained and summarized in Table 5. Using these optimal design data in a theoretical calculation, the resultant curves of the *SWL* with respect to various mufflers are plotted in Fig. 6. As illustrated in Table 5, the resultant SWL with respect to muffler A and B will be reduced from 123 dB(A) to 78.51 dB and 97.52 dB.

2. Discussion

To achieve a sufficient optimization, the selection of the appropriate *SA* parameter set is essential. As indicated in Table 3, the best *SA* set with respect to muffler A (a one-chamber perforated muffler with sound absorbing wool) at the targeted pure tone of 1700 Hz has been shown. Table 4 indicates that for a fixed targeted frequency (1700 Hz), the acoustical performance will be improved when the length of the dissipative muffler, the porosity of the inner duct, the diameter of the perforated hole on the inner duct, the diameter of the inner duct, and the acoustical flowing resistance increase. As revealed in Fig. 5, the *STL* is precisely maximized at the desired frequency when using the best design data. Moreover, it is obvious that the acoustical performance of muffler A (with sound absorbing wool) is superior to that of the muffler B (without sound absorbing wool) in the higher frequency of 1700 Hz.

In dealing with a higher frequency noise emitted from a blower, the optimal design of two kinds of mufflers within a limited space has been discussed and shown in Table 5 and Fig. 6. As indicated in Table 5, the noise reduction with respect to muffler A and muffler B is 44.49 dB and 25.48 dB. Moreover, as indicated in Fig. 6, muffler A having the widest band and highest *STL* is superior to muffler B in the higher frequency region. As indicated in Figs. 5 and 6, muffler B having narrow-band *STL* characteristics will be suitable for eliminating the pure tone and lower frequency noise. However, in dealing with a broadband's noise, muffler B is insufficient. It has been seen that the overall acoustical performance will be substantially improved using muffler A where the sound absorbing wool is added. Moreover, the acoustical performance will be improved when the acoustical flowing resistance is increased.

To appreciate the influence of the *STL* with respect to other parameters such as Mach number(M), diameter of the perforated hole (dH), porosity(η), ratio of the perforated tube's length (L_2/L_o), expansion ratio(d_1/D_o), and the acoustical flowing resistance of the wool (σ_{fr}) for a one-chamber perforated muffler filled with wool, the trend of the *STL* profiles for an optimized muffler at 1700 Hz has been calculated by varying the value of each parameter (M, dH, η, L_2/L_o, d_1/D_o, and σ_{fr}). As indicated in Figs. 7-9, it is obvious that the *STL* is inversely proportional to the Mach number(M) & the

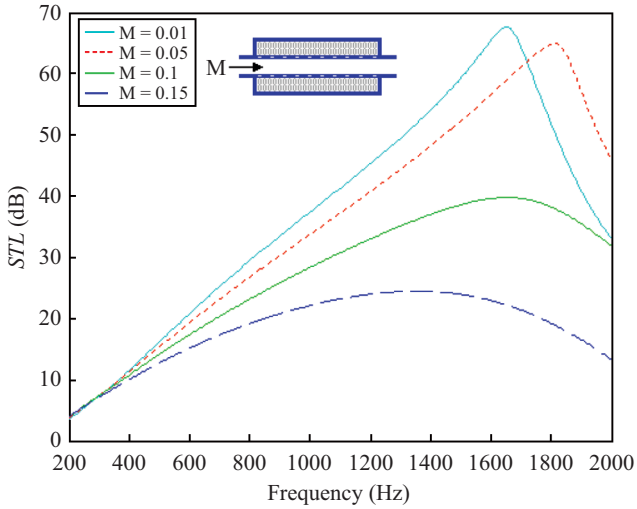

Fig. 7. The *STL* with respect to frequencies at various *M*.

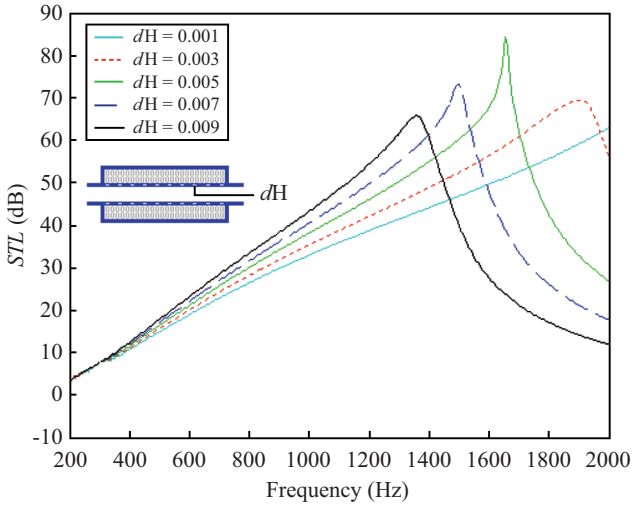

Fig. 10. The *STL* with respect to frequencies at various *d*H (= RT_3).

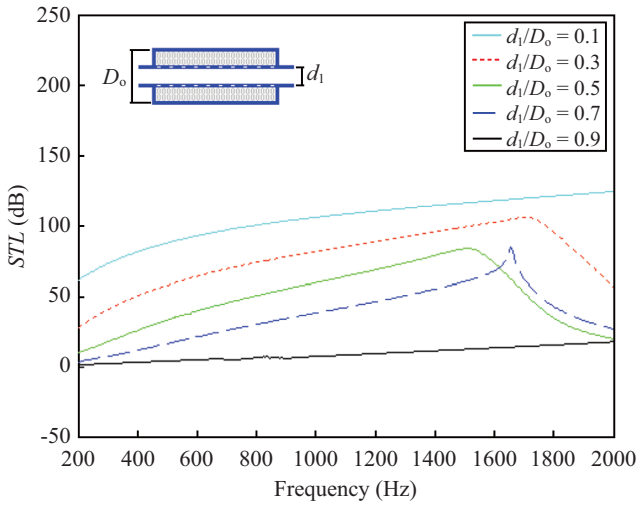

Fig. 8. The *STL* with respect to frequencies at various d_1/D_o (= RT_5).

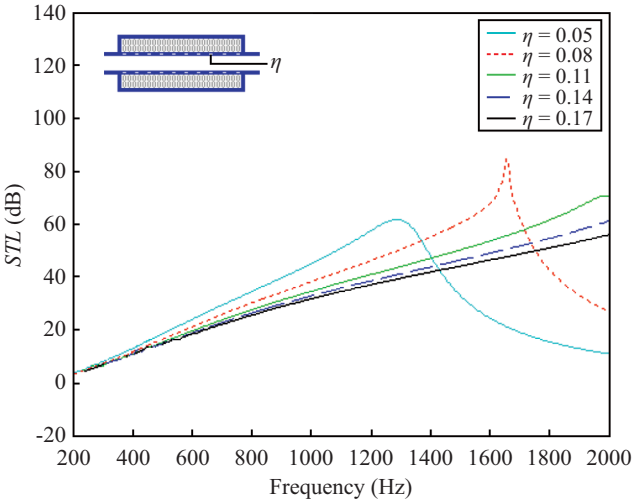

Fig. 11. The *STL* with respect to frequencies at various η (= RT_4).

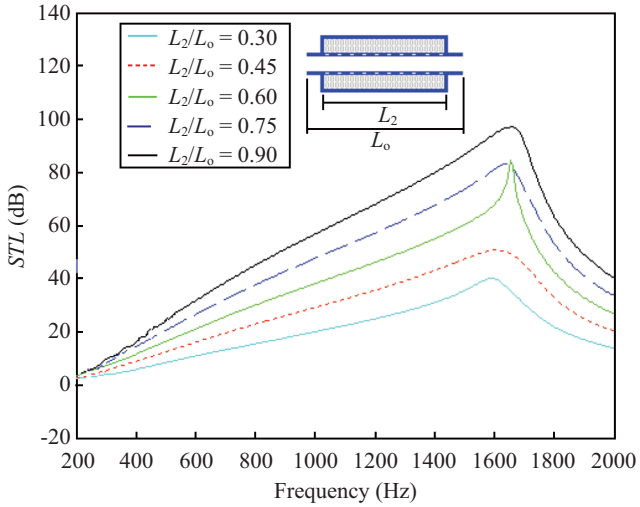

Fig. 9. The *STL* with respect to frequencies at various L_2/L_o (= RT_1).

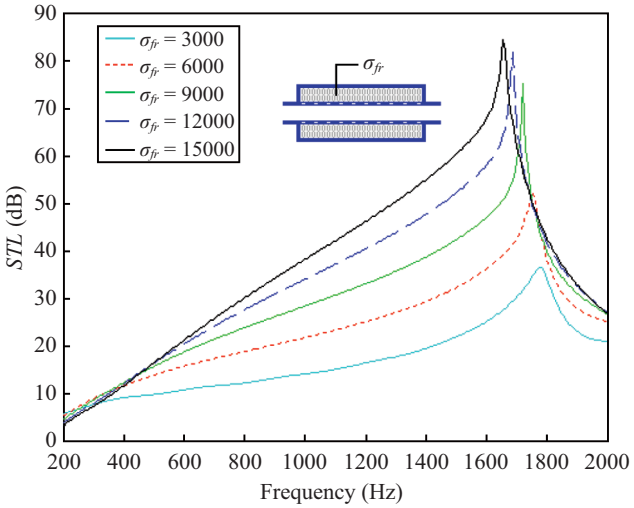

Fig. 12. The *STL* with respect to frequencies at various σ_{fr} (= RT_2).

expansion ratio (d_1/D_o) and proportional to the ratio of the perforated tube's length (L_2/L_o). Additionally, Fig. 10 indicates that the peak frequency will decrease when the diameter of the perforated hole (dH) increases. However, as indicated in Fig. 11, the peak frequency will increase when the porosity of the perforated tube (η) increases. Moreover, as indicated in Fig. 12, the peak frequency will shift to the left and the related *STL* will increase when the acoustical flowing resistance of the wool (σ_{fr}) increases.

Consequently, Mach number (M), diameter of the perforated hole (dH), porosity (η), ratio of the perforated tube's length (L_2/L_o), expansion ratio (d_1/D_o), and the flowing resistance of the wool (σ_{fr}) play essential roles in eliminating the noise level in mufflers.

VII. CONCLUSION

It has been shown that the one-chamber perforated mufflers with/without sound absorbing wool in conjunction with a *SA* optimizer can be easily and efficiently optimized under space limits by using a numerical decoupling technique, plane wave theory, as well as a four-pole transfer matrix. As indicated in Table 3, eight kinds of *SA* parameters (*kk*, *iter*) play essential roles in the solution's accuracy during *SA* optimization. As indicated in Fig. 5, the *STL* is precisely maximized at the desired frequency; therefore, the tuning ability established by adjusting the design parameters of the mufflers is reliable. As indicated in Figs. 5 and 6 muffler B having narrow-band *STL* characteristics will be suitable for eliminating the pure tone and lower frequency noise. However, in dealing with a broadband's noise, muffler B is insufficient. It has been seen that the overall acoustical performance will be substantially improved using muffler A where the sound absorbing wool is added. Moreover, the acoustical performance will be improved when the acoustical flowing resistance of the wool (σ_{fr}) & the ratio of the perforated tube's length (L_2/L_o) & the porosity (η) are increased and the Mach number (M) & the expansion ratio (d_1/D_o) are decreased. Furthermore, the peak frequency of the STL will decrease when the diameter of the perforated hole (dH) increases. Consequently, muffler A having sound absorbing wool which results in the widest band and highest *STL* is superior to muffler B. This approach used for the optimal design of the *STL* proposed in this study is easy and quite effective.

NOMENCLATURE

This paper is constructed on the basis of the following notations:

C_i	coefficients in function ($\Gamma_i = C_i e^{\gamma_i x}$)
C_o	sound speed (m s^{-1})
$\tilde{C}_o$	sound speed in a wool (m s^{-1})
$d\mathrm{H}_i$	the diameter of a perforated hole on the i-th inner tube (m)
D_i	diameter of the i-th perforated tubes (m)
D_o	diameter of the outer tube (m)
f	cyclic frequency (Hz)
iter	maximum iteration
j	imaginary unit
k	wave number $(=\frac{\omega}{c_o})$
$\tilde{k}(\omega)$	the wave number for the wool
kk	cooling rate in *SA*
L_o	total length of the muffler (m)
M	mean flow Mach number
OBJ	objective function (dB)
p	acoustic pressure (Pa)
$\bar{p}_i$	acoustic pressure at the i-th node (Pa)
$pb(T)$	transition probability
Q	volume flow rate of venting gas (m^3 s^{-1})
S_i	section area at the i-th node (m^2)
STL	sound transmission loss (dB)
SWLO	unsilenced sound power level inside the muffler's inlet (dB)
SWL_T	overall sound power level inside the muffler's output (dB)
t_i	the thickness of the i-th inner perforated tube (m)
TS_{ij}	components of four-pole transfer matrices for an acoustical mechanism with straight ducts
TPR_{ij}	components of a four-pole transfer matrix for an acoustical mechanism with an empty perforated chamber
TPD_{ij}	components of a four-pole transfer matrix for an acoustical mechanism with a perforated chamber filled with sound absorbing wool
T^*_{ij}	components of a four-pole transfer system matrix
u	acoustic particle velocity (m s^{-1})
$\bar{u}_i$	acoustic particle velocity at the i-th node (m s^{-1})
u	acoustical particle velocity passing through a perforated hole from the i-th node to the j-th node (m s^{-1})
V_1	mean flow velocity at the inner perforated tube (m s^{-1})
V_2	mean flow velocity at the outer tube (m s^{-1})
ρ_o	air density (kg m^{-3})
$\tilde{\rho}_o$	wool density (kg m^{-3})
ρ_i	acoustical density at the i-th node
ξ_i	specific acoustical impedance of the i-th inner perforated tube
η_i	the porosity of the i-th inner perforated tube.
α_∞	the structure factor for the wool
σ_{fr}	the acoustical flowing resistance for the wool
γ_i	i-th eigen value of $[\mathrm{N}]_{4\times4}$
ω	angular velocity (= $2\pi f$)
$[\Omega]_{4\times4}$	the model matrix formed by four sets of eigen vectors $\Omega_{4\times1}$ of $[\mathrm{N}]_{4\times4}$

ACKNOWLEDGMENTS

The author acknowledges the financial support of the National Science Council (NSC99-2221-E-235-001, Taiwan, ROC).

APPENDIX A - TRANSFER MATRIX OF A PERFORATED CHAMBER FILLED WITH SOUND ABSORBING WOOL

As indicated in Fig. 1, the perforated resonator is composed of an inner perforated tube and an outer resonating chamber. Based on Sullivan and Crocker's derivation [22], the continuity equations and momentum equations with respect to inner and outer tubes at nodes 2 and 2 are listed below.

Inner tube:

continuity equation:

$$V\frac{\partial \rho_2}{\partial x}+\rho_o\frac{\partial u_2}{\partial x}+\frac{4\rho_o}{D_1}u+\frac{\partial \rho_2}{\partial t}=0 \tag{A1}$$

momentum equation:

$$\rho_o\left(\frac{\partial}{\partial t}+V\frac{\partial}{\partial x}\right)u_2+\frac{\partial p_2}{\partial x}=0 \tag{A2}$$

Outer tube:

continuity equation:

$$\tilde{\rho}\frac{\partial u_{2a}}{\partial x}-\frac{4D_1\tilde{\rho}}{D_o^2-D_1^2}u+\frac{\partial \rho_{2a}}{\partial t}=0 \tag{A3}$$

momentum equation:

$$\tilde{\rho}\frac{\partial u_{2a}}{\partial t}+\frac{\partial p_{2a}}{\partial x}=0 \tag{A4}$$

Assuming that the acoustic wave is a harmonic motion

$$P(x,t)=P(x)\cdot e^{j\omega t} \tag{A5}$$

under the isentropic processes in ducts, it yields

$$P(x)=\rho(x)\cdot c_o^2 \tag{A6}$$

Assuming that the perforation along the inner tube is uniform ($d\xi/dx$ = 0), the acoustic impedance of the perforation ($\rho_o\, c_o\, \xi$) is

$$\rho_o c_o \xi=\frac{p_2(x)-p_{2a}(x)}{u(x)} \tag{A7}$$

where ξ is the specific acoustical impedance of the perforated tube.

The empirical formulations developed by Sullivan [22] and Rao [16] for the perforates with and without mean flow are adopted in this study.

For perforates with stationary medium, we have

$$\xi=[0.006+jk(t+0.75dH)]/\eta_{1A} \tag{A8a}$$

For perforates with grazing flow, we have

$$\xi_{1A}=[0.514D_1M_1/(L_C\eta)+j0.95k(t+0.75dH)]/\eta \tag{A.8b}$$

where dH is the diameter of a perforated hole on inner tube, t is the thickness of an inner perforated tube, and η is the porosity of the perforated tube.

Plugging Eqs. (A5)-(A7) into Eqs. (A1)-(A4) and Eliminating u_2 and u_{2a}, we have

$$\left[(1-M^2)\frac{d^2}{dx^2}-2jMk\frac{d}{dx}+k^2\right]p_2 -\frac{4}{D_1\xi}\left[M\frac{d}{dx}+jk\right](p_2-p_{2a})=0 \tag{A9}$$

$$\left[\frac{d^2}{dx^2}+\tilde{k}^2\right]p_{2a}+j\frac{4kD_1\tilde{\rho}}{(D_o^2-D_1^2)\xi\rho_0}(p_2-p_{2a})=0 \tag{A10}$$

where $M_2=\dfrac{V_2}{c_o}$

Alternatively, Eqs. (A9) and (A10) can be expressed as

$$p_2''+\alpha_1 p_2'+\alpha_2 p_2+\alpha_3 p_{2a}'+\alpha_4 p_{2a}=0 \tag{A11a}$$

$$\alpha_5 p_2'+\alpha_6 p_2+p_{2a}''+\alpha_7 p_{2a}'+\alpha_8 p_{2a}=0 \tag{A11b}$$

where

$$\alpha_1=-\frac{jM}{1-M^2}\left(2k-j\frac{4}{D_1\xi}\right);\ \alpha_2=\frac{1}{1-M^2}\left(k^2-j\frac{4k}{D_1\xi}\right);$$

$$\alpha_3=\frac{M}{1-M^2}\cdot\frac{4}{D_1\xi};\ \alpha_4=\frac{j}{1-M^2}\cdot\frac{4k}{D_1\xi};\ \alpha_5=0;$$

$$\alpha_6=\frac{j4kD_1\tilde{\rho}}{(D_o^2-D_1^2)\xi\rho_o};\ \alpha_7=0;\ \alpha_8=\tilde{k}^2-\frac{j4kD_1\tilde{\rho}}{(D_o^2-D_1^2)\xi\rho_o};\ k=\frac{\omega}{c}; \tag{A11c}$$

Let

$$p_2^{'} = \frac{dp_2}{dx} = y_1,\ p_{2A}^{'} = \frac{dp_{2a}}{dx} = y_2,\ p_2 = y_3,\ p_{2A} = y_4 \tag{A12}$$

According to Eqs. (A11) and (A12), the new matrix between {y'} and {y} is

$$\begin{bmatrix} y_1^{'} \\ y_2^{'} \\ y_3^{'} \\ y_4^{'} \end{bmatrix} = \begin{bmatrix} -\alpha_1 & -\alpha_3 & -\alpha_2 & -\alpha_4 \\ -\alpha_5 & -\alpha_7 & -\alpha_6 & -\alpha_8 \\ 1 & 0 & 0 & 0 \\ 0 & 1 & 0 & 0 \end{bmatrix} \begin{bmatrix} y_1 \\ y_2 \\ y_3 \\ y_4 \end{bmatrix} \tag{A13a}$$

which can be briefly expressed as

$$\{y^{'}\} = [\mathrm{N}]\{y\} \tag{A13b}$$

Let

$$\{y\} = [\Omega]\{\Gamma\} \tag{A14a}$$

which is

$$\begin{bmatrix} dp_2/dx \\ dp_{2A}/dx \\ p_2 \\ p_{2A} \end{bmatrix} = \begin{bmatrix} \Omega_{1,1} & \Omega_{1,2} & \Omega_{1,3} & \Omega_{1,4} \\ \Omega_{2,1} & \Omega_{2,2} & \Omega_{2,3} & \Omega_{2,4} \\ \Omega_{3,1} & \Omega_{3,2} & \Omega_{3,3} & \Omega_{3,4} \\ \Omega_{4,1} & \Omega_{4,2} & \Omega_{4,3} & \Omega_{4,4} \end{bmatrix} \begin{bmatrix} \Gamma_1 \\ \Gamma_2 \\ \Gamma_3 \\ \Gamma_4 \end{bmatrix} \tag{A14b}$$

$[\Omega]_{4\times4}$ is the model matrix formed by four sets of eigen vectors $\Omega_{4\times1}$ of $[\mathrm{N}]_{4\times4}$.

Combining Eq. (A14) with Eq. (A13) and then multiplying $[\Omega]^{-1}$ by both sides yields

$$[\Omega]^{-1}[\Omega]\{\Gamma^{'}\} = [\Omega]^{-1}[\mathrm{N}][\Omega]\{\Gamma\} \tag{A15a}$$

Set

$$[\chi] = [\Omega]^{-1}[\mathrm{N}][\Omega] = \begin{bmatrix} \gamma_1 & 0 & 0 & 0 \\ 0 & \gamma_2 & 0 & 0 \\ 0 & 0 & \gamma_3 & 0 \\ 0 & 0 & 0 & \gamma_4 \end{bmatrix} \tag{A15b}$$

where γ_i is the eigen value of [N]

Eq. (A13) can be thus rewritten as

$$\{\Gamma^{'}\} = [\chi]\{\Gamma\} \tag{A16}$$

Obviously, Eq. (A15) is a decoupled equation. The related solution obtained is

$$\Gamma_i = \Gamma_{i} = C_i e^{r_i x} \tag{A17}$$

Plugging Eq. (A17) into Eq. (A14b) and doing a rearrangement, we have

$$\begin{bmatrix} p_2(x) \\ p_{2a(x)} \\ \dfrac{dp_2(x)}{dx} \\ \dfrac{dp_{2a}(x)}{dx} \end{bmatrix} = \begin{bmatrix} \Omega_{3,1}e^{r_1 x} & \Omega_{3,2}e^{r_2 x} & \Omega_{3,3}e^{r_3 x} & \Omega_{3,4}e^{r_4 x} \\ \Omega_{4,1}e^{r_1 x} & \Omega_{4,2}e^{r_2 x} & \Omega_{4,3}e^{r_3 x} & \Omega_{4,4}e^{r_4 x} \\ \Omega_{1,1}e^{r_1 x} & \Omega_{1,2}e^{r_2 x} & \Omega_{1,3}e^{r_3 x} & \Omega_{1,4}e^{r_4 x} \\ \Omega_{2,1}e^{r_1 x} & \Omega_{2,2}e^{r_2 x} & \Omega_{2,3}e^{r_3 x} & \Omega_{2,4}e^{r_4 x} \end{bmatrix} \begin{bmatrix} C_1 \\ C_2 \\ C_3 \\ C_4 \end{bmatrix} \tag{A18}$$

From Eqs. (A2) and (A4), it becomes

$$\rho_o c_o u_2 = -\frac{1}{jk + M\gamma_i}\frac{dp_2}{dx};\ \tilde{\rho}\tilde{c}u_{2a} = -\frac{1}{j\tilde{k}}\frac{dp_{2a}}{dx} \tag{A19}$$

Plugging Eq. (A19) into Eq. (A18) yields

$$\begin{bmatrix} p_2(x) \\ p_{2a}(x) \\ \rho_o c_o u_2(x) \\ \tilde{\rho}\tilde{c}u_{2a}(x) \end{bmatrix} = \begin{bmatrix} \mathrm{H}_{1,1} & \mathrm{H}_{1,2} & \mathrm{H}_{1,3} & \mathrm{H}_{1,4} \\ \mathrm{H}_{2,1} & \mathrm{H}_{2,2} & \mathrm{H}_{2,3} & \mathrm{H}_{2,4} \\ \mathrm{H}_{3,1} & \mathrm{H}_{3,2} & \mathrm{H}_{3,3} & \mathrm{H}_{3,4} \\ \mathrm{H}_{4,1} & \mathrm{H}_{4,2} & \mathrm{H}_{4,3} & \mathrm{H}_{4,4} \end{bmatrix} \begin{bmatrix} C_1 \\ C_2 \\ C_3 \\ C_4 \end{bmatrix} \tag{A20}$$

Substituting two cases of x = 0 and x = Lc into Eq. (A20) yields

$$\begin{bmatrix} p_2(0) \\ p_{2a}(0) \\ \rho_o c_o u_2(0) \\ \tilde{\rho}\tilde{c}u_{2a}(0) \end{bmatrix} = [\mathrm{A}] \begin{bmatrix} p_2(L_C) \\ p_{2a}(L_C) \\ \rho_o c_o u_2(L_C) \\ \tilde{\rho}\tilde{c}u_{2a}(L_C) \end{bmatrix} \tag{A21a}$$

where

$$[\mathrm{A}] = [\mathrm{H}(0)][\mathrm{H}(L_C)]^{-1} \tag{A21b}$$

The boundary conditions for the inner tube are

$$\frac{p_{2a}(0)}{-u_{2a}(0)} = -j\tilde{\rho}\tilde{c}\cot(\tilde{k}L_A) \quad \text{at x} = 0 \tag{A22a}$$

$$\frac{p_{2a}(L_C)}{u_{2a}(L_C)} = -j\tilde{\rho}\tilde{c}\cot(\tilde{k}L_B) \quad \text{at x} = L_C \tag{A22b}$$

Plugging Eq. (A22) into Eq. (A21) yields

$$\begin{bmatrix} p_2(0) \\ \rho_o c_o u_2(0) \end{bmatrix} = \begin{bmatrix} TPD_{1,1} & TPD_{1,2} \\ TPD_{2,1} & TPD_{2,2} \end{bmatrix} \begin{bmatrix} p_{2A}(L_C) \\ \rho_o c_o u_{2A}(L_C) \end{bmatrix} \tag{A23a}$$

The simplified alternative form is

$$\begin{bmatrix} \bar{p}_2 \\ \rho_o c_o \bar{u}_2 \end{bmatrix} = \begin{bmatrix} TPD_{1,1} & TPD_{1,2} \\ TPD_{2,1} & TPD_{2,2} \end{bmatrix} \begin{bmatrix} \bar{p}_3 \\ \rho_o c_o \bar{u}_3 \end{bmatrix} \quad \text{(A23b)}$$

where

$$\bar{p}_2 = p_2(0); \bar{u}_2 = u_2(0); \bar{p}_3 = p_{2a}(L_C); \bar{u}_3 = u_{2a}(L_C); \quad \text{(A23c)}$$

REFERENCES

1. Chiu, M. C. and Chang, Y. C., "Numerical studies on venting system with multi-chamber perforated mufflers by GA optimization," *Applied Acoustics*, Vol. 69, No. 11, pp. 1017-1037 (2008).
2. Chiu, M. C., Chang, Y. C., and Yeh, L. J., "Numerical assessment of optimal one-chamber perforated mufflers by using GA method," *Material Science Forum*, Vol. 594, pp. 368-376 (2008).
3. Cummings, A. and Chang, I. J., "Internal mean flow effects on the characteristics of bulk-reacting liners in circular ducts," *Acustica*, Vol. 64, pp. 169-178 (1987).
4. Cummings, A. and Chang, I. J., "Sound attenuation of a finite length dissipative flow duct silencer with internal mean flow in the absorbent," *Journal of Sound and Vibration*, Vol. 127, pp. 1-17 (1988).
5. Jayaraman, K. and Yam, K., "Decoupling approach to modeling perforated tube muffler component," *Journal of the Acoustical Society of America*, Vol. 69, No. 2, pp. 390-396 (1981).
6. Kirkpatrick, S., Gelatt, C. D., and Vecchi, M. P., "Optimization by simulated annealing," *Science*, Vol. 220, No. 4598, pp. 671-680 (1983).
7. Ko, S. H., "Theoretical analyses of sound attenuation in acoustically lined flow ducts separated by porous splitters (rectangular, annular and circular ducts)," *Journal of Sound and Vibration*, Vol. 39, pp. 471-487 (1975).
8. Lee, I. J., *Acoustic Characteristics of Perforated Dissipative and Hybrid Silencers*, Doctor Thesis, Ohio State University (2005).
9. Metropolis, N., Rosenbluth, A. W., Rosenbluth, M. N., Teller, A. H., and Teller, E., "Equation of state calculations by fast computing machines," *Journal of Chemical Physics*, Vol. 21, No. 6, pp. 1087-1092 (1953).
10. Morse, P. M., "The transmission of sound inside pipes," *Journal of the Acoustical Society of America*, Vol. 11, pp. 205-210 (1939).
11. Munjal, M. L., *Acoustics of Ducts and Mufflers with Application to Exhaust and Ventilation System Design*, John Wiley & Sons, New York (1987).
12. Munjal, M. L., "Analysis and design of pod silencers," *Journal of Sound and Vibration*, Vol. 262, pp. 497-507 (2003).
13. Munjal, M. L., Rao, K. N., and Sahasrabudhe, A. D., "Aeroacoustic analysis of perforated muffler components," *Journal of Sound and Vibration*, Vol. 114, No. 2, pp. 173-188 (1987).
14. Peat, K. S., "A numerical decoupling analysis of perforated pipe silencer elements," *Journal of Sound and Vibration*, Vol. 123, No. 2, pp. 199-212 (1988).
15. Peat, K. S., "A transfer-matrix for an absorption silencer element," *Journal of Sound and Vibration*, Vol. 146, pp. 353-360 (1991).
16. Rao, K. N. and Munjal, M. L., "A generalized decoupling method for analyzing perforated element mufflers," *Proceedings of the 1984 Nelson Acoustics Conference*, Wisconsin (1984).
17. Scott, R. A., "The propagation of sound between walls of porous material," *Proceedings of the Physics Society*, Vol. 58, pp. 358-368 (1946).
18. Selamet, A., Lee, I. J., and Huff, N. T., "Acoustic attenuation of hybrid silencers," *Journal of Sound and Vibration*, Vol. 262, pp. 509-527 (2003).
19. Selamet, A., Lee, I. J., Ji, Z. L., and Huff, N. T., "Acoustic attenuation performance of perforated concentric absorbing silencers," *SAE Noise and Vibration Conference and Exposition*, SAE Paper No. 2001-01-1435 (2001).
20. Sullivan, J. W., "A method of modeling perforated tube muffler components I: Theory," *Journal of the Acoustical Society of America*, Vol. 66, pp. 772-778 (1979).
21. Sullivan, J. W., "A method of modeling perforated tube muffler components II: Applications," *Journal of the Acoustical Society of America*, Vol. 66, pp. 779-788 (1979).
22. Sullivan, J. W. and Crocker, M. J., "Analysis of concentric tube resonators having unpartitioned Cavities," *Journal of the Acoustical Society of America*, Vol. 64, pp. 207-215 (1978).
23. Thawani, P. T. and Jayaraman, K., "Modeling and applications of straight-through resonators," *Journal of the Acoustical Society of America*, Vol. 73, No. 4, pp. 1387-1389 (1983).
24. Wang, C. N., *The Application of Boundary Element Method in the Noise Reduction Analysis for the Automotive Mufflers*, Doctor Thesis, Taiwan University, Taipei, Taiwan (1992).
25. Xu, M. L., Selamet, A., Lee, I. J., and Huff, N. T., "Sound attenuation in dissipative expansion chambers," *Journal of Sound and Vibration*, Vol. 272, pp. 1125-1133 (2004).